Journal of Materials Science: Materials in Medicine (2019) 30:78
https://doi.org/10.1007/s10856-019-6279-x

S.I.: BIOFABRICATION AND BIOINKS FOR TISSUE ENGINEERING

Original Research

Development of mussel-inspired 3D-printed poly (lactic acid) scaffold grafted with bone morphogenetic protein-2 for stimulating osteogenesis

Cheng-Hsin Cheng[1,2,3] · Yi-Wen Chen[4,5] · Alvin Kai-Xing Lee[6,7] · Chun-Hsu Yao[8,9,10,11] · Ming-You Shie[6,11,12]

Received: 30 April 2018 / Accepted: 7 June 2019 / Published online: 20 June 2019

Abstract

3D printing is a versatile technique widely applied in tissue engineering due to its ability to manufacture large quantities of scaffolds or constructs with various desired architectures. In this study, we demonstrated that poly (lactic acid) (PLA) scaffolds fabricated via fused deposition not only retained the original interconnected microporous architectures, the scaffolds also exhibited lower lactic acid dissolution as compared to the freeze-PLA scaffold. The 3D-printed scaffolds were then grafted with human bone morphogenetic protein-2 (BMP-2) via the actions of polydopamine (PDA) coatings. The loading and release rate of BMP-2 were monitored for a period of 35 days. Cellular behaviors and osteogenic activities of co-cultured human mesenchymal stem cells (hMSCs) were assessed to determine for efficacies of scaffolds. In addition, we demonstrated that our fabricated scaffolds were homogenously coated with PDA and well grafted with BMP-2 (219.1 ± 20.4 ng) when treated with 250 ng/mL of BMP-2 and 741.4 ± 127.3 ng when treated with 1000 ng/mL of BMP-2. This grafting enables BMP-2 to be released in a sustained profile. From the osteogenic assay, it was shown that the ALP activity and osteocalcin of hMSCs cultured on BMP-2/PDA/PLA were significantly higher when compared with PLA and PDA/PLA scaffolds. The methodology of PDA coating employed in this study can be used as a simple model to immobilize multiple growth factors onto different 3D-printed scaffold substrates. Therefore, there is potential for generation of scaffolds with different unique modifications with different capabilities in regulating physiochemical and biological properties for future applications in bone tissue engineering.

✉ Chun-Hsu Yao
chyao@mail.cmu.edu.tw

✉ Ming-You Shie
eric@mail.cmu.edu.tw

[1] Graduate Institute of Clinical Medical Science, China Medical University, Taichung, Taiwan

[2] Department of Neurosurgery, Tainan Municipal An-Nan Hospital-China Medical University, Tainan, Taiwan

[3] Department of Neurosurgery, China Medical University Hospital, China Medical University, Taichung, Taiwan

[4] Graduate Institute of Biomedical Sciences, China Medical University, Taichung, Taiwan

[5] 3D Printing Medical Research Institute, Asia University, Taichung, Taiwan

[6] 3D Printing Medical Research Center, China Medical University Hospital, Taichung, Taiwan

[7] School of Medicine, China Medical University, Taichung, Taiwan

[8] Department of Biomedical Imaging and Radiological Science, China Medical University, Taichung, Taiwan

[9] School of Chinese Medicine, China Medical University, Taichung, Taiwan

[10] Biomaterials Translational Research Center, China Medical University Hospital, Taichung, Taiwan

[11] Department of Bioinformatics and Medical Engineering, Asia University, Taichung, Taiwan

[12] School of Dentistry, China Medical University, Taichung, Taiwan

Graphical Abstract

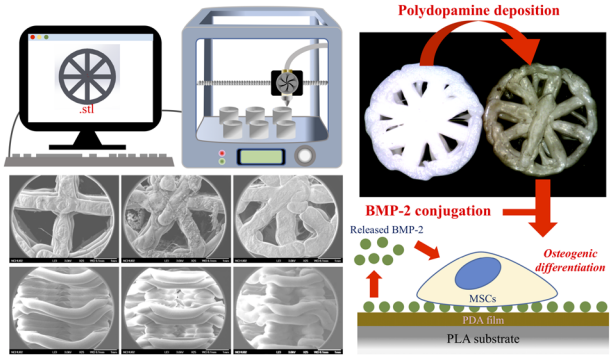

1 Introduction

An aging population brings about a whole spectrum of orthopaedic diseases such as osteoporosis and increased fracture risk, thus this had led to an increment in cases of bone grafting procedures worldwide [1]. Shortage of bone graft supply had motivated and led researchers to look for alternatives such as exploring for viable bone substitutes. Therefore, there was also an exponential increase in bone tissue engineering research and related studies. An ideal bone substitute must have the ability to deliver cells, to support differentiation of host cells as well as biocompatible with host tissues and have osteoconductive and osteoinductive capabilities. In addition, an ideal scaffold ought to have controlled biodegradability in order to balance bone formation and scaffold degeneration [2]. The final goal of tissue engineering is to fabricate substitutes to assist regeneration of new functional tissue via biological, engineering and apt design cues [3]. Currently, there are several different techniques and materials available for bone grafting such as autologous, allograft and xenograft bone grafts and bioceramics materials such as hydroxyapatite, calcium sulphate and polycaprolactone [4, 5]. Additive manufacturing had developed and evolved over the past few decades and current technology allows researchers to print 3D scaffolds with desired specific micro-architectures solely by inputting computer aided design files which are processed from medical images such as CT scans or MRI [6, 7]. In addition, this layer-by-layer manufacturing technology of 3D printing can produce scaffolds of higher porosity traits with full interconnectivity between pores. This was almost impossible and unimaginable during the era of traditional scaffold manufacturing [8, 9]. Printable polymers such as polycaprolactone (PCL), poly(lactide) (PLA), poly(ethylene glycol)-diacrylate are currently being used for biomedical applications [10, 11].

PLA has been proven to possess excellent biocompatibility and biodegradability in a wide range of orthopaedic applications [12]. Indeed, a plethora of innovative designs and concepts have been developed using PLA and further studies showed that PLA exhibited excellent biocompatibility with bone [13]. Most importantly, PLA is a US Food and Drug Administration approved biomaterial. In addition to synthetic materials, natural polymers such as collagen, chitosan, and alginate are also widely used in tissue engineering and 3D printing, [14, 15]. However, amongst all the biodegradable materials, PLA still remains as one of the most promising and common bio-polymer [16, 17] that is widely used in textile, pharmaceutical (drug-carriers) and implant applications. Recent studies indicated that PLA-based biomaterials are also widely utilized in automotive, communication and electronic industries due to their high durability. A bone defect study has also shown that PLA can accelerate bone healing in tibias of rats and induce higher bone formation when compared to non-treated controls [18]. In spite of these promising studies, PLA is still a hydrophobic material that is unable to promote high cell-cell interaction and this greatly limits its potential for biomaterial applications [19].

In recent years, scientists discovered that 3,4-dihydroxy-L- phenylalanine (DOPA) had a huge role to play in providing robust adhesion support between mussels and rocks [20]. Dopamine (DA) is found to have catechol functional groups that can be utilized to increase polymerization when exposed to a certain pH (through oxidative transformation from catechol to quinone) [21]. Such polymerization allowed a layer of poly-dopamine (PDA) to be coated onto the surface of mussels which then has potential affinities for various kinds of bioactive molecules such as polysaccharides, peptides, enzymes, and growth factor to attach to [22, 23]. For in-vitro settings, this material-independent PDA coating can be easily and quickly achieved through base-triggered oxidation and polymerization of DA. This

PDA ad-layer can be used to serve as a platform for post-modifications, including spontaneous deposition of metal and bioceramics, as well as covalent immobilization of several protein adhesive proteins [24, 25]. Modifications of surface hydrophilicity and attachment of bioactive functional groups were shown to enhance cellular behaviors on self-assembled PDA/calcium phosphate composite nano-layer [26].

Several growth factors have been proven as potential therapeutic agents for hard-tissues formation [27, 28]. Notably, bone morphogenetic protein-2 (BMP-2) is crucial for bone formation in the first stage of healing after bone injury and is also known to be able to enhance osteogenic differentiation of stem cells [29]. Specifically, BMP-2 was found to enhance cell proliferation and osteogenic differentiation in bone marrow mesenchymal cells [29]. BMP-2 signaling plays an important role in the control of osteoprogenitor cells differentiation and knockout of BMP-2 gene in mice resulted in decreased bone marrow stromal cell osteogenic differentiation and therefore affected bone formation. Several signal transduction pathways were activated when BMP-2 binds to BMP-2 receptor (BMP-2R), such as receptor phosphorylation of intrinsic tyrosine residues which includes mitogen-activated protein kinases (MAPK) and phosphatidylinositol 3-kinase (PI3K) [30].

This present study aims to explore the differences between the mechanical and biological properties of 3D-printed PLA scaffolds and traditional free-extraction PLA scaffolds, which were seldom discussed in recent papers. In addition, proliferation, osteogenesis and angiogenesis of mesenchymal stem cells were investigated to evaluate for the efficacy of PDA and BMP-2 surface modifications. This study aims to value add to current bone regeneration studies by evaluating the true potentials of 3D-printed scaffolds and to determine its potential application as a material for future bone grafts.

2 Materials and methods

2.1 Preparation of freeze-extraction PLA scaffolds

PLA (Mw: ~80000–100000 g/mole, Polyscience) was dissolved in dioxane to form a 3 wt% polymer solution. The polymer solution was set in a glass petri dish and frozen at −20 °C. The solvent in the frozen solution was subsequently extracted via freeze-extraction [18]. The end-product is named as freeze-PLA scaffold.

2.2 Fabrication of the 3DP PLA scaffolds

The 3D-PLA scaffolds (4-3D-PLA, 6-3D-PLA, and 8-3D-PLA) were designed using SpaceClaim 2014 CAD package (SpaceClaim Corporation, Concord, MA) and saved as stereolithography (stl) file thus allowing direct import into the printer software. In the printer, a cartridge was installed to supply the feedstock PLA filament into the fused deposition modeling (FDM) 3D printer (Prusa I3), and the melted PLA filament was extruded through the 0.2 mm diameter stainless-steel nozzle onto a heated printing plate. The layer thickness of the scaffolds was set to 0.2 mm to allow for fine details and good print quality. The samples were cylindrical in shape with a diameter of 6 mm and a height of 8 mm.

2.3 Mechanical property analysis and characterization

The micromorphology of the various scaffolds was observed using scanning electron microscope (SEM). Resistance to mechanical compression was tested on a SHIMADZU (AG-10KNIS) testing machine with a 10 kN load cell at room temperature according to the guidelines as stated in ASTMD5024-95a. The crosshead speed was set at 0.5 mm/min, and the load was applied until the sample was compressed up to 70% original height. The compressive modulus was calculated as the slope of the initial linear section of the stress–strain curve. The compressive strength was determined by the maximum point of the stress–strain curve. The reported data was the average of five samples ($N = 5$).

2.4 Porosity measurement

The porosity was measured by using specific gravity method. Each set contains five samples ($N = 5$) and were done at room temperature. Each sample was weighed (ms) and immersed in ethanol (m0). The samples were individually weighed (m1) once the pores were fully soaked with ethanol. The rest of the ethanol and specific gravity bottle was weighed and categorized as m2. Porosity was determined and recorded according to this formula: Porosity = (m1-m2-ms)/(m0-m2).

2.5 Swelling ratio measurements

The samples were immersed in Sorensen's buffer solution. After soaking for 3, 6, 12, 24, and 48 h at room temperature, the samples were removed from the Sorensen's buffer solution, wiped with filter paper to remove excess liquid and subsequently weighed (Wt). These samples were then frozen, dried (using the same aforementioned procedures), and weighed (W0). The swelling ratio (ΔW%) was determined using this formula: $\Delta W\ (\%) = (Wt - W0)/W0 \times 100\ (\%)$.

2.6 Degradation rate and pH value

The degradation rate was evaluated according to ISO 10993 guidelines. All scaffolds were irradiated by gamma ray (10 kGy) before being placed in covered plastic tubes filled with 3 mL Sorensen's buffer solution and subsequently incubated at 37 °C. After soaking for different time-points, the samples were retrieved from the buffer and frozen-dried. The degree of degradation was determined by monitoring for weight change of the scaffolds. The scaffolds were weighed both before (W0) and after (Wt) immersion using a balance. The weight loss percentage (ΔW%) was then calculated according to this formula: $\Delta W\% = (W0 - Wt)/W0 \times 100\%$. The degradation rate for each scaffold then was determined by dividing its ΔW% with soaking duration. In addition, variations in the pH value of different scaffolds during the degradation process was measured with a pH meter. Five parallel specimens were performed with every group.

2.7 Lactate concentration

After disinfection with 60 °C gamma ray irradiation (10 kGy), the samples were placed in covered plastic tubes filled with 3 mL of Sorensen's buffer solution and incubated at 37 °C. After soaking for 4, 8, 12, 16, 20 and 24 weeks, the soaking solution was collected to measure for the amount of residual lactate. This was done by using colorimetric analysis with lactate colorimetric assay kit (K627-100, BioVision) according to the manufacturer's instructions. pH change in the incubation Sorensen buffer was recorded at the end of each sampling time point.

2.8 The effect of scaffolds extracts on MG-63 proliferation

Human osteoblast-like cell line MG-63 (BCRC, number 60279) was obtained from Food Industry Research and Development Institute (FIRDI, Hsinchu, Taiwan). To evaluate biocompatibility, MG-63 cells were seeded onto 24 wells plates at a concentration of 1×10^4 cells/well and cultured with various scaffold extracts for 3 days. For the MTT assay, the medium was replaced with 20 μL/well of MTT solution (5 mg/ml) and 180 μL/ well of culture medium and incubated at 37 °C for 4 h to allow formation of formazan crystals. The solution was then removed and 200 μL/well of acid propan-2-ol (0.04 M HCl in isopropanol) was added to all wells and mixed thoroughly to dissolve the dark-blue crystals. After 5 min at room temperature to ensure all crystals were dissolved, the plates were read using ELISA reader with a test wavelength of 570 nm against a reference wavelength of 650 nm. The number of viable cells was determined by converting the optical density (OD) values from the MTT assay into numbers of cells based on a standard curve.

2.9 Poly(dopamine) and BMP-2 coating

The deposition of dopamine (H8502, Sigma) onto 8-3D-PLA scaffold were conducted via direct immersion coating. All scaffolds were rinsed with deionized water and immersed into a dopamine solution (2 mg/mL in 10 mM Tris, pH 8.5) and placed into a 25 rpm shaker at room temperature for different time-points. All scaffolds were then rinsed with deionized water. The dopamine-coated PLA scaffolds were subsequently immersed in BMP-2 solution (250, 500, 1000 ng/mL in 10 mM Tris-HCl buffer, PeproTech) and incubated at 37 °C overnight.

2.10 Quantification of BMP-2 on the scaffolds

The amounts of BMP-2 on the scaffolds was analyzed using enzyme linked immunoassay (DY355, R&D system). Calibration curve were obtained using different concentrations of BMP-2 solution. Subsequently, BMP-2 capture antibody was added and allowed to react for 24 h, followed by addition of 100 μL/well residual solution for 90 min, rhBMP-2 antibody detection solution for 90 min, avidin-HRP solution for 30 min and TMB solution for 15 min. The abovementioned reaction was terminated using 2N HCl and a spectrometer (SpectraMAX M2e. Molecular Device, Sunnyvale, CA, USA) was used to measure absorbance at absorption wavelength of 405 nm. Interpolation method was applied to the ELISA calibration curve to obtain residual content of BMP-2 solution. The BMP-2 immobilized concentration is calculated as follows: Immobilized concentration of BMP-2 = BMP-2 concentration before reaction - BMP-2 concentration after reaction.

2.11 BMP-2 release profile

Immobilized amount and long-term release kinetics of BMP-2 was indirectly measured using enzyme-linked immunosorbent assay. After incubation with PBS for various time-points, BMP-2 in the supernatant was measured using an ELISA kit. Daily collected supernatants were stored at −70 °C until the day of ELISA experiment. All the ELISA experiments were performed according to the manufacturer's protocol, and sample absorbance was measured using a spectrophotometer at 450 nm with 540 nm used for λ correction.

2.12 Stem cells culture

Human mesenchymal stem cells (hMSCs) purchased from Cambrex Inc. (Charles City, IA, USA) were cultured as monolayers in low-glucose DMEM (Biological Industries) with 10% FBS and 1% PS at 37 °C with 5% CO_2 in a humidified environment. Medium was replaced every

2–3 days. For osteogenesis differentiation assay, the medium was replaced with osteogenic differentiation media with 10% FBS, 1% PS, 50 µg/mL ascorbic acid, 0.01 M glycerol-2-phosphate, and 10^{-7} M dexamethasone after 12 h. The osteogenesis assay was prepared as described in the section below.

2.13 Cell morphology

After 6 h and 7 days of hMSCs (1×10^5 cells/scaffold) post seeding on scaffolds, the specimens were washed three times with 1 × PBS, fixed with 2 % glutaraldehyde and dehydrated in graded ethanol. The morphology of the attached cells was observed using scanning electron microscopy (SEM, S-3000; Hitachi).

2.14 Osteogenesis differentiation

hMSCs were seeded onto the 24 wells at a concentration of 1×10^4 cells/well and cultured with extracts for 7 and 18 days. Subsequently, the medium was removed and the wells were washed three times with PBS. 200 µL/well of ALP reagent (SIGMAFASTTM pNPP substrate, Simga N2770) was added to the wells in a dark environment for 30 min, followed by measurement of absorption by using a ELISA reader at 405 nm wavelength.

In addition, the osteocalcin assay was used to quantify osteocalcin production using enzyme-linked immunosorbent assay (ELISA, Biomedical Technologies, Inc., USA). The assay was added to the ELISA sample-buffer and homogenized via sonication after 14 days of culture. The cell lysates (100 µL) were placed into a 96-well plate and incubated at 4 °C for 24 h. After washing with PBS twice, 100 µL of an osteocalcin anti-serum and 100 µL of donkey anti-goat IgG peroxidase was added to each well and incubated for 2 h at room temperature. After washing with PBS twice, 100 µL of the substrate solution was added to the wells and incubated for 30 min at room temperature, followed by addition of 100 µL of an acidic stop solution to stop the reactions. The absorbance was measured at 450 nm, and the OC expression level by the cells was determined based on an OC standard prepared in the range of 0.1–2 ng/mL.

2.15 Statistical analysis

A one-way analysis of the variance statistical data was used to evaluate the significance of the differences between the means in the measured data. A Scheffe's multiple comparison test was used to determine the significance of the deviations in the data for each specimen. In all cases, the results were considered statistically significant with a p value < 0.05.

3 Results

3.1 Characterization of PLA scaffolds

Special designed 3D-printed PLA scaffolds were used for this study. The uppermost layer of the scaffolds was specially designed to section the top of the scaffolds into four, six and eight equal parts that were then named as 4-3D-PLA, 6-3D-PLA and 8-3D-PLA respectively (Fig. 1). The control group used in this study was freeze-dried PLA scaffolds (freeze-PLA) with irregular pore size fabricated

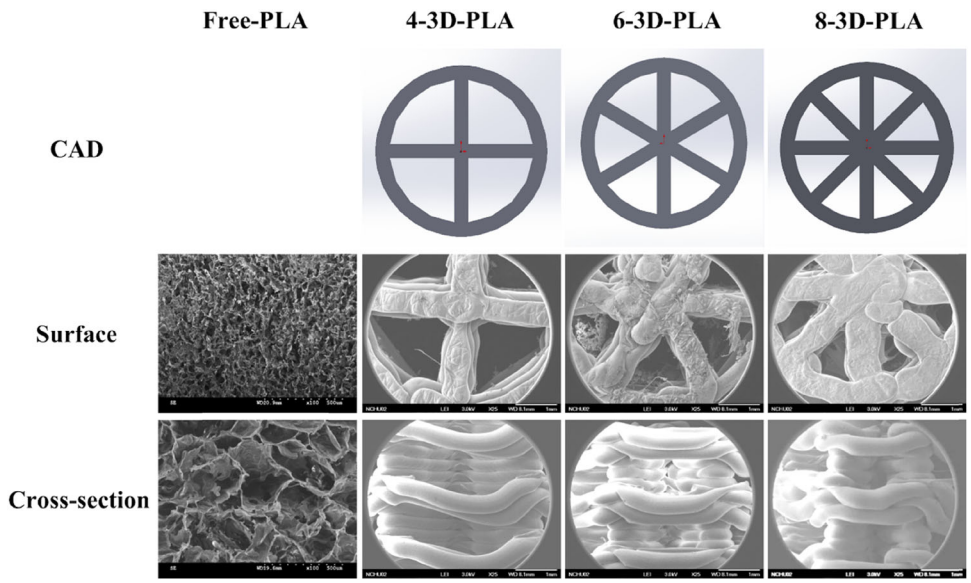

Fig. 1 The CAD and microstructure of freeze-PLA scaffold and 3D printed-PLA scaffold with different structure

Table 1 The line width, pore size and porosity of PLA scaffold with different structure

Scaffold	Line width (μm)	Pore size (μm)	Porosity (%)
Freeze-PLA	–	Surface: 55 ± 17 Cross section: 159 ± 73	91 ± 2.5[a]
4-3D-PLA	290 ± 36	1711 ± 199	90 ± 0.9[a]
6-3D-PLA	275 ± 32	1125 ± 179	88 ± 2.3[a]
8-3D-PLA	283 ± 30	817 ± 80	80 ± 2.0[b]

Values not sharing a common letter are significantly different at $P < 0.05$

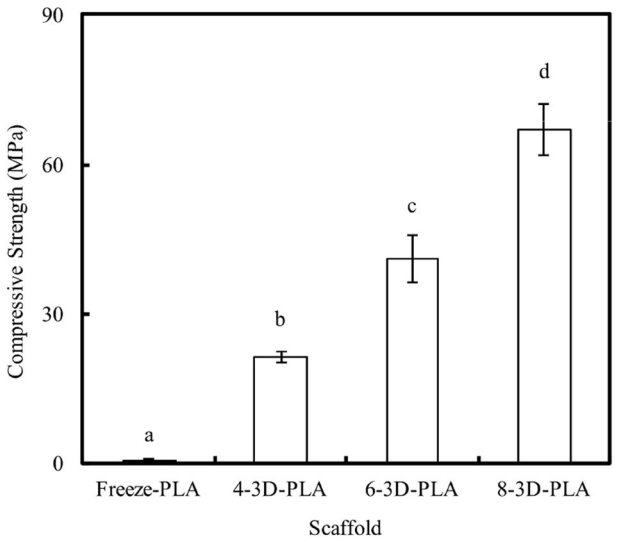

Fig. 2 The mechanical properties of various PLA scaffold. Values not sharing a common letter are significantly different at $P < 0.05$

using traditional methods. For this study, the surface and inner pore sizes of freeze-PLA were found to be 55 μm and 159 μm respectively. On the other hand, there were no significant differences ($P > 0.05$) between the widths of PLA in each 3D-printed scaffold (Table 1). Several studies had pointed out that scaffolds with higher porosity and interconnected channels of defined diameters between 300 to 900 μm were optimal for bone tissue engineering. The porosity of Freeze-PLA, 4-3D-PLA, 6-3D-PLA, and 8-3D-PLA was found to be 90.9 ± 2.5%, 90.1 ± 0.9%, 87.7 ± 2.3% and 80 ± 2.0%, respectively (Table 1). There were no significant differences in porosity between Freeze-PLA, 4-3D-PLA and 6-3D-PLA. However, the porosity of 8-3D-PLA scaffold were significantly lower than the others ($P < 0.01$). It was also shown that mechanical tests were significantly higher in all 3D-PLA scaffolds as compared to the Freeze-PLA scaffolds (Fig. 2). In addition, the results showed that mechanical properties increased with the increment of printed lines per layer. Moreover, Fig. 3 indicated that the swelling ratio of 6-3D-PLA and 8-3DPLA were lower than that of freeze-PLA. With relation to

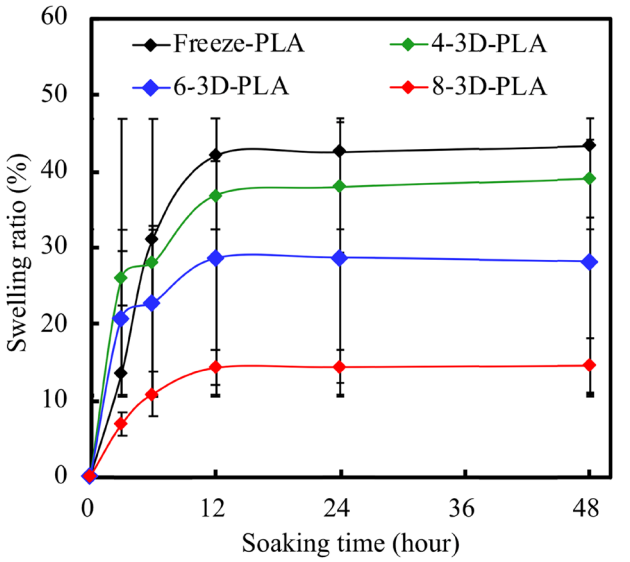

Fig. 3 The swelling ration for various PLA scaffold during immersion in PBS for 48 h

porosity, the surface contact area is higher in freeze-PLA and 4-3D-PLA as compared to the rest.

3.2 Immersion studies of PLA scaffolds

Figure 4a showed the weight loss (due to degradation) of various PLA scaffolds when immersed in PBS solution at 37 °C for 24 weeks. The weight loss profile of all 3D-printed specimens were similar at the beginning. Degradation rate of freeze-PLA scaffolds rapidly increased and peaked after 24 weeks (5.25%). Degradation rate was higher in the freeze-PLA group as compared to all the 3D-printed groups. Throughout the degradation period, presence of lactic acid (0.11 ± 0.01 nmole/μL) was detected in the freeze-PLA group (Fig. 4b). In addition, the concentration of lactic acid released from freeze-PLA gradually increased as time goes by. On the contrary, the concentration of lactic acid in 3DP scaffolds were significantly lower as compared to freeze-PLA scaffolds (0.05 nmole/μL). The 3DP scaffolds exhibited constant and gradual release of lactic acid. The profile of lactic acid release was similar to the degradation assay of scaffolds. Figure 4c shows the change of pH value at different time points of immersion. The pH value of freeze-PLA immersed in PBS for 4, 16, 20, and 24 weeks were 7.17, 7.09, 7.00, and 6.92, respectively.

3.3 Cytotoxicity

MTT assay was used to assess for indirect cytotoxicity of the degraded by products of PLA (Fig. 5). There were significantly higher cell counts in the freeze-PLA and 8-3D PLA group when compared to the control group, thus

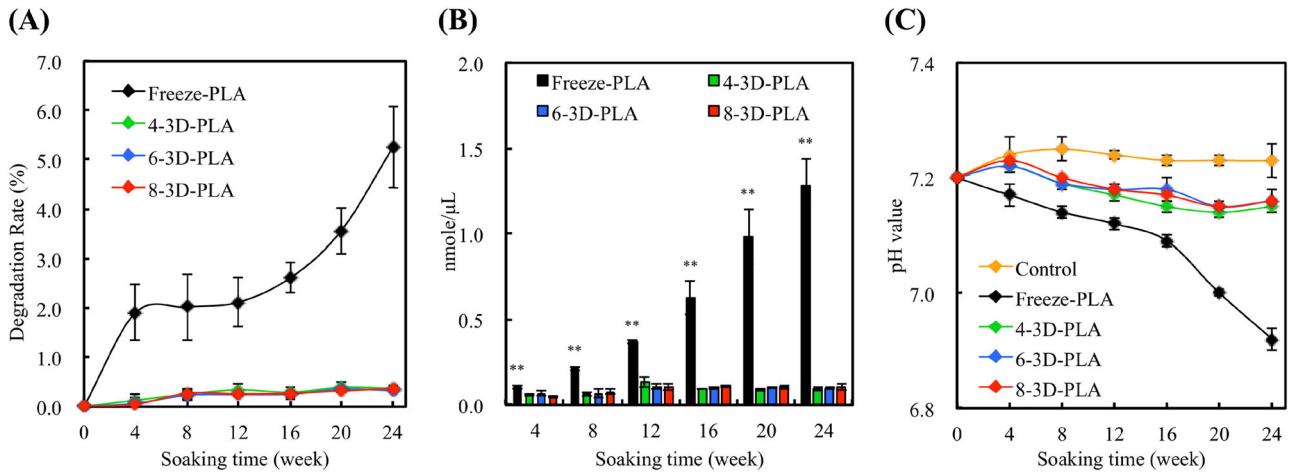

Fig. 4 **a** The degradation ratio, **b** the concentration of lactate from PLA scaffold, and **c** pH value of various PLA scaffold immersed in buffer solution for different times. Asterisk indicates a significant difference ($P < 0.01$) compared to 3D-printed scaffold

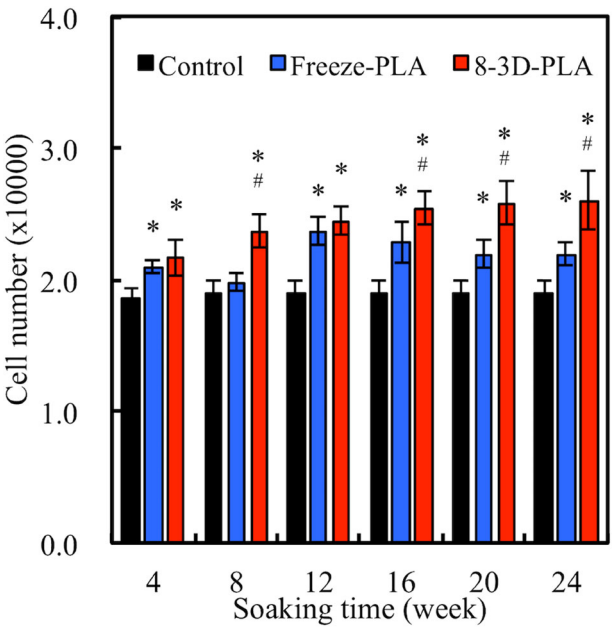

Fig. 5 The cytotoxicity of the MG63 cells cultured with various extract medium. The extract medium contained freeze-PLA and 8-3D-PLA after immersed at 4th, 8th, 12th, 16th, 20th and 24th weeks. The control group was medium without extract. Asterisk indicates a significant difference ($P < 0.05$) compared to control. Pound sign indicates a significant difference ($P < 0.05$) compared to freeze-PLA

indicating that the PLA degraded by-products were non-toxic in nature. In addition, cell proliferation in the 8-3D PLA groups were significantly higher than the freeze-PLA scaffold. Therefore, we hypothesized that cell proliferation might be limited by the lower pH caused by the degraded by products of the freeze-PLA scaffold. Thus, we concluded that 3D-printed PLA scaffolds exhibited enhanced biocompatibility as there were no toxic solvents (e.g., dioxane) used during manufacturing.

3.4 Quantification of coated PDA

Images of the PDA coated PLA scaffolds were shown in Fig. 6a and it can be seen that the scaffolds were cylindrical in shape, were porous and had interconnected networks. PDA coating causes a color change of the scaffold from white to shades of deep uniform brown. In addition, Fig. 6b showed a distinct difference between the elemental composition of PLA scaffolds before and after PDA coating. There was a significant increase in nitrogen content and a significant decrease in the carbon content after 24 h.

3.5 BMP-2 releasing profile

Based on the above results, we chose 24 h as the optimal time for subsequent PDA coating. In order to evaluate for the effectiveness of BMP-2 grafting, PDA-coated scaffolds were immersed in different concentrations of BMP-2 and amount of unattached BMP2 was quantified to assess for grafting efficiency of the PDA-coated. The amounts of BMP-2 grafted on the BMP250, BMP500, and BMP1000 groups were found to be 219.1 ± 20.4 ng, 375.4 ± 44.3 ng, and 741.4 ± 127.3 ng, respectively (Fig. 7a). This showed that the level of BMP-2 coating on the surface of the PLA scaffold was proportional to the concentration of BMP-2. We also performed a release test of BMP2 from the BMP250, BMP500, and BMP1000 groups for 35 days (Fig. 7b). In all groups, there was an initial burst release of BMP-2 at day 1, with 60.1ng, 54.3 and 60.5 ng BMP-2 released from BMP250, BMP500 and BMP1000 respectively. Following which, BMP-2/PDA/PLA scaffolds exhibited

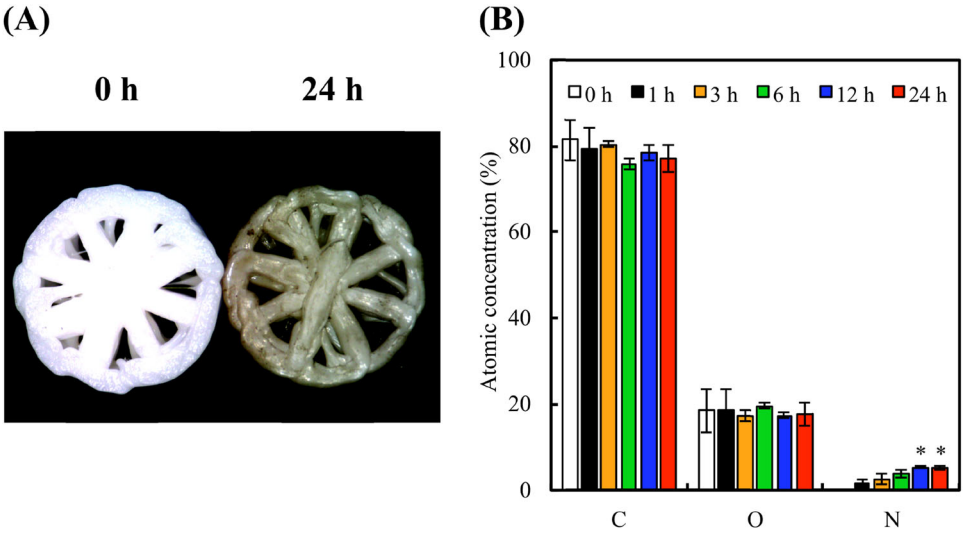

Fig. 6 **a** The photograph of PDA-coated PLA scaffold. **b** XPS high-resolution spectra obtained different atom on PLA scaffolds after coating with dopamine for different time-points. Asterisk indicates a significant difference ($p < 0.05$) compared to 0 h

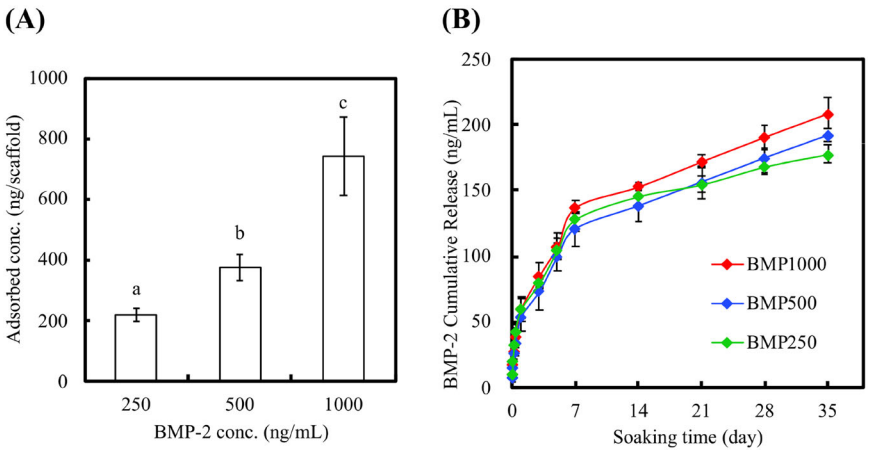

Fig. 7 **a** The concentration of BMP-2 adsorbed on the PDA-coated 3D PLA scaffold. Values not sharing a common letter are significantly different at $p < 0.05$. **b** The accumulated level of BMP-2 released from the PDA-coated PLA scaffold after immersion in PBS at 37 °C for different time points

sustained released of BMP-2 for up to 35 days. The final accumulated amounts of BMP-2 release from BMP250, BMP500, and BMP1000 for 35 days were 177.8 ± 7.1, 192.3 ± 5.6, and 209 ± 11.7 ng respectively. These values suggested that approximately 70% of BMP2 was released from the PDA-coated PLA scaffold.

3.6 Cell morphology

The cell morphology of hMSCs cultured on 3D printed scaffolds in the groups of PLA, PDA/PLA, BMP-2/PDA/PLA were observed using SEM at 6 h and 7 days (Fig. 8). At 6 h, the cells were found to be barely adhered onto surfaces and were not well spread based on their cellular morphology. From the SEM images, the cells were polygonal in shape and exhibited little pseudopodium properties on the surface of PDA/PLA and BMP-2/PDA/PLA scaffolds. After 7 days of culture, obvious pseudopodium and spindle-like cell morphology could be observed in all scaffolds. In the BMP-2/PDA/PLA scaffolds, there were more evident spindle-shaped cells which could imply that might be higher cell transformation and growth.

3.7 Osteogenesis differentiation

ALP levels of hMSCs are used as early-stage markers of osteogenesis differentiation. ALP assay results (Fig. 9a) indicated that hMSCs cultured with various modified scaffolds had significantly higher levels of ALP than those without modifications and this can be attributed to the excellent biological behavior induced by BMP-2 release from the scaffolds at all time-points. After 18 days, there were a significant ($P < 0.05$) increase of 2.11- and 1.26-times of ALP activity on BMP-2/PDA/PLA as compared to PLA and PDA/PLA scaffold respectively. It was clear that the response of hMSCs to BMP-2 might be due to the sustained and constant presence of BMP-2. The early induction of BMP-2 also provided a cellular basis for the implementation of the subsequent osteogenic effect at the later stage. The expression of OC was quantified by ELISA

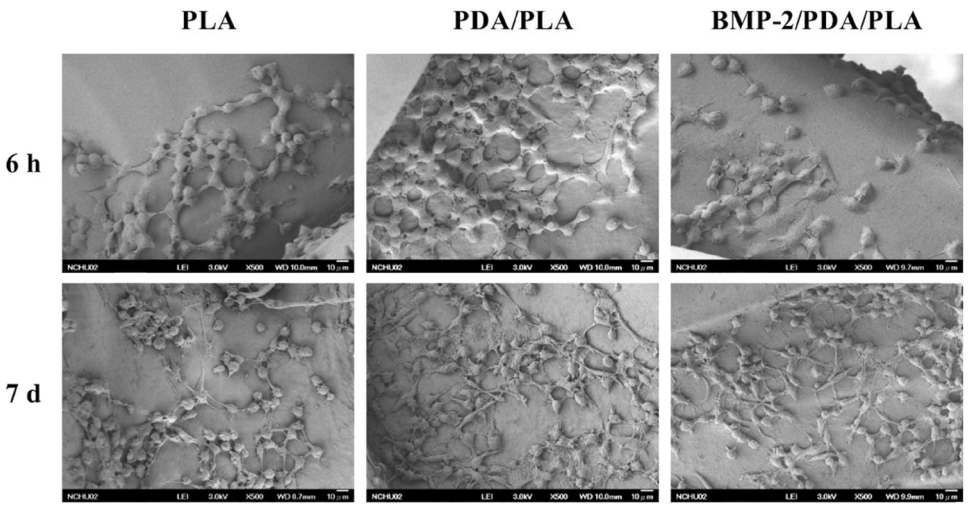

Fig. 8 The morphology of hMSCs cultured on PLA, PDA/PLA, and BMP-2/PDA/PLA scaffold for 6 h and 7 days

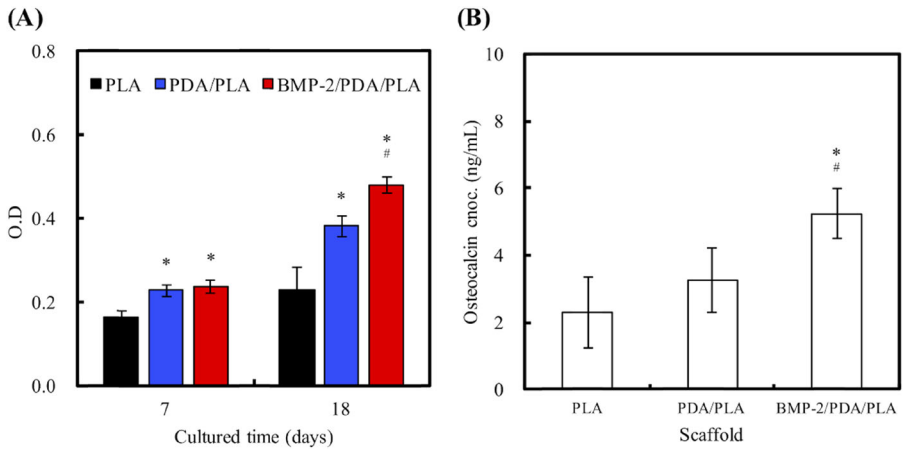

Fig. 9 **a** ALP activity of HMSC cultured on PLA, PDA/PLA, and BMP-2/PDA/PLA scaffold for 7 and 18 days. **b** OC concentration of HMSC cultured on scaffold for 18 days. Asterisk indicates a significant difference ($P < 0.05$) compared to PLA. Pound sign indicates a significant difference ($P < 0.05$) compared to PDA/PLA

to further investigate the promotional effects of BMP-2/PDA/PLA on osteogenic differentiation at later-stages (Fig. 9b).

4 Discussion

The final goal of tissue engineering is to fabricate substitutes to assist regeneration of new functional tissue via biological, engineering and apt design cues [3]. It was reported that biological factors had a larger role to play in facilitating bone regeneration as compared to the scaffolds itself [31, 32]. In a recent study, 3D printing technique was used to fabricate an ideal porous bioscaffold with specific control of architectures matching anatomical shapes and thus making it more ideal forclinical applications [33, 34]. Furthermore, these specific bioscaffold architectures have been shown to significantly influence bone regeneration and scaffold degradation [4, 35].

Traditional methods such as porogen templating, solvent casting and freeze drying were unable to provide us with well-controlled and reproducible microarchitectures [8, 36]. In this sense, 3D printing technology is a more superior technology as compared to traditional methods. Several studies have pointed out that scaffolds with high porosity and interconnected channels of defined diameters between 300 to 900 μm were optimal for bone tissue engineering. Such microarchitectures parameters were optimal as it has a high surface area-to-volume ratio to allow higher rates of mass transfer, cell in-growth and vascularization [1]. However, the interconnectivity and porosity of scaffolds has an absolute relationship with the mechanical properties of scaffolds [37]. Consequently, there would be decreased porosity with the increment of printed lines per layer. It was previously reported that higher porosity may decrease the mechanical strength of the scaffold [37]. The human cortical bone has a reported Young's modulus between the range of 1 to 20 GPa and a strength range of 1 to 100 MPa and

cancellous (trabecular) bone of Young's modulus has a reported Young's modulus between the rage of 0.1 to 1.0 GPa and strength range of 1 to 10 MPa [38]. Despite the wide range of these reported mechanical strength of bones, these values act as a guide for us to fabricate essential scaffolds that can match the native strengths of bones. Through our study, only the 8-3D PLA scaffold exhibited sufficient mechanical properties for usage as bone substitutes. In addition, the results indicated that the swelling ratio of 6-3D-PLA and 8-3D-PLA were lower than that of freeze-PLA. With relation to porosity, the surface contact area is higher in freeze-PLA and 4-3D-PLA as compared to the rest. This larger surface contact area may cause higher water absorption and thus higher swelling ratio [39]. In a previously reported study, Thomas and Windle's model of Case II diffusion proved that water uptake is highly dependent on the stresses due to polymer swelling. Therefore, water uptake is highly dependent on the mechanical deformation of the glassy region in response to polymer swelling.

The solution tends to infiltrate the inner portion of the scaffold through structural imperfections such as defects and pores and penetrated into the deeper portion of the scaffolds thus resulting in a weakened structure. Depending on the clinical needs, degradation rate of the bone substitutes could be influenced to a certain extent by varying structural and architectural properties [40]. Bone regeneration process such as bone formation and resorption were found to be responsive in certain pH. The pH value of bone interstitial fluid may shift to an alkaline pH during resorption and to an acidic pH during bone regeneration. Some studies analyzed the effects of mid-range pH (ranging from 6.8 to 8.2) on calvaria, tibiae, and osteoblast cell [41]. It was reported that ECM synthesis and osteogenesis-related protein production increased exponentially as pH increases. Therefore, we can infer that acidic environment inhibits differentiation and regeneration of bone tissue [42].

This growth factor release tendency is consistent with previous reports which used PDA to graft drugs onto PLA scaffolds [24]. With regards to release rate of BMP-2 from PDA-coated scaffolds, our findings are consistent with earlier reports and findings made by others [43]. Thus, we hypothesized that the primary and main mechanism of BMP-2 release from pure PLA scaffolds during the first 48 h is via desorption from scaffold surface [44]. BMP-2 release from PDA-coated PLA scaffolds stabilized with sustained immersion. PDA has a catechol side chain which might play a possible role in supporting adsorption sites by providing hydrogen bonding that allows growth factor/PDA coating [45]. Numerous studies had attempted to coat PDA on different surfaces and had also attempted to attach secondary proteins onto PDA and it was reported that the bonds were formed between catechol and quinone groups on PDA and amino or thiol side chains of proteins [45]. Therefore, we hypothesized that BMP1000 scaffold may promote a higher level of osteogenesis as compared to the BMP250 scaffolds due to the higher concentrations of BMP2 release as BMP2 is well known to induce osteogenesis differentiation [46].

In a previous study, we proved that surface modified-PLA materials were able to influence the cellular adhesion and affects cell morphology [47]. These data proved that the PDA/PLA surface immobilized with BMP-2 can efficiently endow the implants with promoted biocompatibilities such as inducing hMSCs adhesion [48]. Studies have shown that addition of extracellular matrix components (e.g., fibronectin) and polycations (e.g., poly-lysine) were able to promote certain cellular behaviors depending on the types of components used [49], but our PDA coating strategy could be used to enhance efficiency of cellular adhesion on different substrates and cell lines. Most importantly, PDA coating alters the surface to become hydrophilic. Such a change may enhance cellular adhesion, thus activating intracellular signal transductions and improving cell proliferation [11]. In addition to PDA coating, the addition of BMP-2 further promotes cell adhesion and proliferation [50]. In previous studies were had proved the mechanical stimuli acted as a regulator of osteogenesis differentiation through BMP2-activitied [51]. Afterwards, the osteogenic-related protein, ALP and OC were dramatically activated and upregulated, which are believed as the very important factors for osteogenesis differentiation. OC secretion were found to correlate to ALP activity. At day 18, higher levels of OC secretion were observed in the BMP-2/PDA/PLA scaffolds as compared to the PLA and PDA/PLA scaffolds. These findings verified that the later release of BMP-2 stimulated the proliferation and maturation of pre-osteoblast formed, thus effectively improving bone-related protein secretion and mineralization [52]. The synergistic osteogenic effects of BMP-2 delivered in the release manner from BMP-2/PDA/PLA scaffold was also illustrated.

5 Conclusions

In this study, we successfully fabricated BMP-2-immobilized on PDA-coated PLA scaffold for bone regeneration applications. The 3D-printed PLA scaffolds not only possessed interconnected microporous architecture but also exhibited lower lactic acid release as compared to the freeze-PLA scaffold. In addition, PDA coating significantly affected the surface properties of the PLA scaffolds as well as effectively allowed grafting and sustained release of BMP2. Moreover, both the initial release burst and sustained release of BMP-2 were beneficial for hMSCs proliferation and osteogenesis differentiation. Based on our study, the PDA coating methods can be used as a simple

model to immobilize BMP-2 onto the 3D-printed scaffold that allowed for the generation of 3D-printed scaffolds with excellent biological properties to regulate cellular behaviors and has a potential to serve as an effective stem cell delivery carrier for future bone tissue engineering.

Acknowledgements The authors acknowledge receipt grants from the Ministry of Science and Technology (MOST 105-2314-B-039-024), China Medical University (CMU 106-S-04, CMU 105-S-17) of Taiwan, and Tainan Municipal An-Nan Hospital-China Medical University (ANHRF104-09).

Compliance with ethical standards

Conflict of interest The authors declare that they have no conflict of interest.

References

1. Sarker B, Li W, Zheng K, Detsch R, Boccaccini AR. Designing porous bone tissue engineering scaffolds with enhanced mechanical properties from composite hydrogels composed of modified alginate, gelatin, and bioactive glass. ACS Biomater Sci Eng. 2016;2:2240–54.
2. Tevlek A, Hosseinian P, Ogutcu C, Turk M, Aydin HM. Bi-layered constructs of poly(glycerol-sebacate)-β-tricalcium phosphate for bone-soft tissue interface applications. Mater Sci Eng C Mater Biol Appl. 2017;72:316–24.
3. Tierney EG, Duffy GP, Hibbitts AJ, Cryan SA, O'Brien FJ. The development of non-viral gene-activated matrices for bone regeneration using polyethyleneimine (PEI) and collagen-based scaffolds. J Control Release. 2012;158:304–11.
4. Bertol LS, Schabbach R, Loureiro Dos Santos LA. Different post-processing conditions for 3D bioprinted α-tricalcium phosphate scaffolds. J Mater Sci Mater Med. 2017;28:168.
5. Chen YW, Wu YH, Shie MY. Characterization of decellularized extracellular matrix on 3d-printed ceramic scaffolds for promoted osteogenesis differentiation. Tissue Eng Part A. 2017;23:S46.
6. Hinton TJ, Hudson A, Pusch K, Lee A, Feinberg AW. 3D printing PDMS elastomer in a hydrophilic support bath via freeform reversible embedding. ACS Biomater Sci Eng. 2016;2:1781–6.
7. Huang A, Jiang Y, Napiwocki B, Mi H, Peng X, Turng LS. Fabrication of poly(ε-caprolactone) tissue engineering scaffolds with fibrillated and interconnected pores utilizing microcellular injection molding and polymer leaching. RSC Adv. 2017;7:43432–44.
8. Liu W, Wang D, Huang J, Wei Y, Xiong J, Zhu W, et al. Low-temperature deposition manufacturing: A novel and promising rapid prototyping technology for the fabrication of tissue-engineered scaffold. Mater Sci Eng C Mater Biol Appl. 2017;70:976–82.
9. Wang Di, Wang Y, Wang J, Song C, Yang Y, Zhang Z, et al. Design and fabrication of a precision template for spine surgery using selective laser melting (SLM). Materials. 2016;9:608.
10. Wu YH, Chiu YC, Lin YH, Ho CC, Shie MY, Chen YW. 3D-printed bioactive calcium silicate/poly-ε-caprolactone bioscaffolds modified with biomimetic extracellular matrices for bone regeneration. Int J Mol Sci. 2019;20:942.
11. Kao CT, Lin CC, Chen YW, Yeh CH, Fang HY, Shie MY. Poly (dopamine) coating of 3D printed poly(lactic acid) scaffolds for bone tissue engineering. Mater Sci Eng C Mater Biol Appl. 2015;56:165–73.
12. Guduric V, Metz C, Siadous R, Bareille R, Levato R, Engel E, et al. Layer-by-layer bioassembly of cellularized polylactic acid porous membranes for bone tissue engineering. J Mater Sci Mater Med. 2017;28:78.
13. Shim JH, Moon TS, Yun MJ, Jeon YC, Jeong CM, Cho DW, et al. Stimulation of healing within a rabbit calvarial defect by a PCL/PLGA scaffold blended with TCP using solid freeform fabrication technology. J Mater Sci Mater Med. 2012;23:2993–3002.
14. Sun X, Cheng L, Zhao J, Jin R, Sun B, Shi Y, et al. bFGF-grafted electrospun fibrous scaffolds via poly(dopamine) for skin wound healing. J Mater Chem B. 2014;2:3636–45.
15. Rajzer I, Menaszek E, Kwiatkowski R, Planell JA, Castaño O. Electrospun gelatin/poly(ε-caprolactone) fibrous scaffold modified with calcium phosphate for bone tissue engineering. Mater Sci Eng C Mater Biol Appl. 2014;44:183–109.
16. Yang F, Murugan R, Wang S, Ramakrishna S. Electrospinning of nano/micro scale poly(L-lactic acid) aligned fibers and their potential in neural tissue engineering. Biomaterials. 2005;26:2603–10.
17. Lin CC, Fu SJ, Lin YC, Yang IK, Gu Y. Chitosan-coated electrospun PLA fibers for rapid mineralization of calcium phosphate. Int J Biol Macromol. 2014;68:39–47.
18. Li J, Xu Q, Teng B, Yu C, Song L, Lai YX, et al. Investigation of angiogenesis in bioactive 3-dimensional poly(d,l-lactide-co-glycolide)/nano-hydroxyapatite scaffolds by in vivo multiphoton microscopy in murine calvarial critical bone defect. Acta Biomater. 2016;42:389–99.
19. Kai D, Liow SS, Loh XJ. Biodegradable polymers for electrospinning: towards biomedical applications. Mater Sci Eng C Mater Biol Appl. 2014;45:659–70.
20. Lee H, Dellatore SM, Miller WM, Messersmith PB. Mussel-inspired surface chemistry for multifunctional coatings. Science. 2007;318:426–30.
21. Cheng YL, Chen YW, Wang K, Shie MY. Enhanced adhesion and differentiation of human mesenchymal stem cell inside apatite-mineralized/poly(dopamine)-coated poly(ε-caprolactone) scaffolds by stereolithography. J Mater Chem B. 2016;4:6307–15.
22. Fu J, Quek KY, Chuah YJ, Lim CS, Fan C, Wang DA. The effects of gelatin–dopamine coating on polydimethylsiloxane substrates on pluripotency maintenance and myocardial differentiation of cultured mouse embryonic stem cells. J Mater Chem B. 2016;4:7961–73.
23. Yu J, Lin YH, Yang L, Huang CC, Chen L, Wang WC, et al. Improved anticancer photothermal therapy using the bystander effect enhanced by antiarrhythmic peptide conjugated dopamine-modified reduced graphene oxide nanocomposite. Adv Healthc Mater. 2017;6:1600804.
24. Yeh CH, Chen YW, Shie MY, Fang HY. Poly(dopamine)-assisted immobilization of Xu Duan on 3D printed poly(lactic acid) scaffolds to up-regulate osteogenic and angiogenic markers of bone marrow stem cells. Materials. 2015;8:4299–315.
25. Sun H, Ai M, Zhu S, Jia X, Cai Q, Yang X. Polylactide–hydroxyapatite nanocomposites with highly improved interfacial adhesion via mussel-inspired polydopamine surface modification. RSC Adv. 2015;5:95631–42.
26. Wu C, Han P, Liu X, Xu M, Tian T, Chang J, et al. Mussel-inspired bioceramics with self-assembled Ca-P/polydopamine composite nanolayer: preparation, formation mechanism, improved cellular bioactivity and osteogenic differentiation of bone marrow stromal cells. Acta Biomater. 2014;10:428–38.
27. Marie PJ, Miraoui H, Sévère N. FGF/FGFR signaling in bone formation: progress and perspectives. Growth Factors. 2012;30:117–23.

28. Marie PJ. Fibroblast growth factor signaling controlling bone formation: an update. Gene. 2012;498:1–4.
29. Bayat M, Shojaei S, Bahrami N, Mohamadnia A, Shojaei P, Bahrami N. Protein engineering of recombinant human bone morphogenetic protein 2 with higher interaction with Ca phosphate based scaffold used for osteogenesis. J Biomed Mater Res Part A. 2017;105:2799–805.
30. Sánchez-Duffhues G, Hiepen C, Knaus P, Dijke ten P. Bone morphogenetic protein signaling in bone homeostasis. Bone. 2015;80:43–59.
31. Wu Y, Lin ZYW, Wenger AC, Tam KC, Tang XS. 3D bioprinting of liver-mimetic construct with alginate/cellulose nanocrystal hybrid bioink. Bioprinting. 2018;9:1–6.
32. Ma Y, Ji Y, Zhong T, Wan W, Yang Q, Li A, et al. Bioprinting-based PDLSC-ECM screening for in vivo repair of alveolar bone defect using cell-laden, injectable and photocrosslinkable hydrogels. ACS Biomater Sci Eng. 2017;3:3534–45.
33. Kang KT, Kim SH, Son J, Lee YH, Chun HJ. Computational model-based probabilistic analysis of in vivo material properties for ligament stiffness using the laxity test and computed tomography. J Mater Sci Mater Med. 2016;27:183.
34. Wongsupa N, Nuntanaranont T, Kamolmattayakul S, Thuaksuban N. Biological characteristic effects of human dental pulp stem cells on poly-ε-caprolactone-biphasic calcium phosphate fabricated scaffolds using modified melt stretching and multilayer deposition. J Mater Sci Mater Med. 2017;28:25.
35. Popov A, Malferrari S, Kalaskar DM. 3D bioprinting for musculoskeletal applications. J 3D Print Med. 2017;1:191–211.
36. Yu GZ, Chou D-T, Hong D, Roy A, Kumta PN. Biomimetic rotated lamellar plywood motifs by additive manufacturing of metal alloy scaffolds for bone tissue engineering. ACS Biomater Sci Eng. 2017;3:648–57.
37. Rustom LE, Boudou T, Nemke BW, Lu Y, Hoelzle DJ, Markel MD, et al. Multiscale porosity directs bone regeneration in biphasic calcium phosphate scaffolds. ACS Biomater Sci Eng. 2016;3:2768–78.
38. Link DP, van den Dolder J, van den Beucken JJ, Wolke JG, Mikos AG, Jansen JA. Bone response and mechanical strength of rabbit femoral defects filled with injectable CaP cements containing TGF-β1 loaded gelatin microparticles. Biomaterials. 2008;29:675–82.
39. Sadat-Shojai M, Khorasani M-T, Jamshidi A. 3-Dimensional cell-laden nano-hydroxyapatite/protein hydrogels for bone regeneration applications. Mater Sci Eng C Mater Biol Appl. 2015;49:835–43.
40. Mohammadkhah A, Marquardt LM, Sakiyama-Elbert SE, Day DE, Harkins AB. Fabrication and characterization of poly-(ε)-caprolactone and bioactive glass composites for tissue engineering applications. Mater Sci Eng C Mater Biol Appl. 2015;49:632–9.
41. Ramp WK, Lenz LG, Kaysinger KK. Medium pH modulates matrix, mineral, and energy metabolism in cultured chick bones and osteoblast-like cells. Bone Miner. 1994;24:59–73.
42. Chen YW, Shen YF, Ho CC, Yu J, Wu YH, Wang K, et al. Osteogenic and angiogenic potentials of the cell-laden hydrogel/mussel-inspired calcium silicate complex hierarchical porous scaffold fabricated by 3D bioprinting. Mater Sci Eng C Mater Biol Appl. 2018;91:679–87.
43. Kao CT, Huang TH, Chen YJ, Hung CJ, Lin CC, Shie MY. Using calcium silicate to regulate the physicochemical and biological properties when using β-tricalcium phosphate as bone cement. Mater Sci Eng C Mater Biol Appl. 2014;43:126–34.
44. Liu CH, Huang TH, Hung CJ, Lai WY, Kao CT, Shie MY. The synergistic effects of fibroblast growth factor-2 and mineral trioxide aggregate on an osteogenic accelerator in vitro. Int Endod J. 2014;47:843–53.
45. Chien CY, Tsai WB. Poly(dopamine)-assisted immobilization of Arg-Gly-Asp peptides, hydroxyapatite, and bone morphogenic protein-2 on titanium to improve the osteogenesis of bone marrow stem cells. ACS Appl Mater Interfaces. 2013;5:6975–83.
46. Lee SJ, Lee D, Yoon TR, Kim HK, Jo HH, Park JS, et al. Surface modification of 3D-printed porous scaffolds via mussel-inspired polydopamine and effective immobilization of rhBMP-2 to promote osteogenic differentiation for bone tissue engineering. Acta Biomater. 2016;40:182–91.
47. Shie MY, Ding SJ. Integrin binding and MAPK signal pathways in primary cell responses to surface chemistry of calcium silicate cements. Biomaterials. 2013;34:6589–606.
48. Huang KH, Chen YW, Wang CY, Lin YH, Wu YH, Shie MY, et al. Enhanced capability of BMP-2-loaded mesoporous calcium silicate scaffolds to induce odontogenic differentiation of human dental pulp cells. J Endod. 2018;44:1677–85.
49. Ku SH, Ryu J, Hong SK, Lee H, Park CB. General functionalization route for cell adhesion on non-wetting surfaces. Biomaterials. 2010;31:2535–41.
50. Reddi AH. Role of morphogenetic proteins in skeletal tissue engineering and regeneration. Nat Biotechnol. 1998;16:247–52.
51. Rodrigues EM, Gomes Cornélio AL, Soares-Costa A, Salles LP, Velayutham M, Rossa-Junior C, et al. An assessment of the overexpression of BMP-2 in transfected human osteoblast cells stimulated by mineral trioxide aggregate and biodentine. Int Endod J. 2017;50:e9–18.
52. Zhang BJ, He L, Han ZW, Li XG, Zhi W, Zheng W, et al. Enhanced osteogenesis of multilayered pore-closed microsphere-immobilized hydroxyapatite scaffold via sequential delivery of osteogenic growth peptide and BMP-2. J Mater Chem B. 2017;5:8238–53.